JOURNAL OF MATERIALS SCIENCE 30 (1995) 2936–2943

Evaluation of a miniaturized disc test for establishing the mechanical properties of low-alloy ferritic steels

V. VORLICEK*, L. F. EXWORTHY, P. E. J. FLEWITT
Nuclear Electric, Technology Division, Berkeley Technology Centre, Berkeley, Gloustershire, UK GLB 9PB

A miniaturized disc test has been used to measure load–displacement curves for a $2\frac{1}{4}$Cr1Mo steel, from which are derived values for the Young's modulus of elasticity, yield stress and ultimate tensile strength over the temperature range −196 to 25 °C. The miniaturized test uses disc specimens 3 mm diameter and 0.25 mm thick and a test jig that applies a load via a 1 mm diameter steel ball at a constant displacement rate. The reproducibility of the method has been determined by testing a large number of the $2\frac{1}{4}$Cr1Mo steel specimens at each temperature considered. Comparisons have been made between analytical and empirical methods of evaluating the tensile yield stress and ultimate tensile strength from the measured load–displacement data. In addition, consideration has been given to the total energy to fracture, K^*, and the variation with temperature which confirms a transition from low-energy cleavage to high-energy ductile fracture.

1. Introduction

The exposure of operating gas-cooled nuclear electrical power generating plant to neutron irradiation can lead to a change in the mechanical properties of the steels used in the construction of the reactor core and the containing pressure vessel. The neutron irradiation degrades the mechanical properties as a result of the dynamic interaction between dislocations, defect clusters and impurity or solute elements which raise the yield strength and increase the brittle to ductile transition temperature of the material [1]. Of particular interest are the changes to the mechanical properties of the submerged arc-weld metal that is used in the construction of the Magnox steel reactor pressure vessels. Here the response is attributed to the copper content derived from the coating on the welding consumable and also there are changes which have been related to the higher impurity element content, in particular phosphorus [1–3].

As a consequence, a variety of techniques has been adopted to measure the changes in the mechanical properties of steels associated with exposure to neutron irradiation [4]. However, because of the irradiation volume constraints associated with testing larger specimens of these materials, the developments have extended to methods that use small-sized specimens. The volume constraints arise from (a) difficulties associated with testing larger volumes of active material, (b) the limitation, in some circumstances, on the volume of test material that can be exposed to the irradiation environment, and (c) the volume of material that can be extracted from critical locations of operating plant. In particular, variants of the ball punch test have been applied to assess the deformation and fracture properties of these materials [5]. With respect to the deformation characteristics, the properties that have been derived include elastic modulus [5], ductility [6], load–deflection behaviour [7] and biaxial stress–strain behaviour to obtain mechanical properties equivalent to a conventional uniaxial tensile test [8–10]. However, it is in the area of fracture properties and, specifically, the brittle-to-ductile fracture transition temperature that there is a particular need to obtain data [1]. In this respect, Baik *et al.* [11] and Mao *et al.* [12] demonstrated that a ball punch test applied to specimens of 10 mm × 10 mm and 1 mm thickness provides a measure of the brittle-to-ductile transition temperature which can then be related empirically to the Charpy transition temperature. As a consequence, there has been a series of papers published which describe developments of ball punch specimen technology to obtain fracture energy and thereby values of fracture toughness, such as J_{IC} and K_{IC}. The need to obtain such mechanical property data on irradiated material has led Misawa *et al.* [13], McNancy *et al.* [14] and, more recently, Kameda and Mao [15] to extend the technique to testing 3 mm diameter disc specimens to measure a range of mechanical and fracture properties. This has been referred to variously as a super small punch test or a miniaturized disc test; we adopt the latter terminology.

In an earlier report, Exworthy [16] presented results of transition curves for tests conducted on 8 mm diameter and 0.5 mm thick Ducol W30 and low-alloy

* *Permanent address*: Czech Technical University of Prague, Charles Square No. 13, Prague 2, Czech Republic.

0022–2461

TABLE I Chemical analysis of the 2¼Cr1Mo steel (wt %)

C	Mn	S	P	Si	Cr	Ni	Mo	Sn	As	Sb	Fe
0.081	0.45	0.01	0.007	0.28	2.27	0.15	1.00	0.077	0.006	0.02	bal

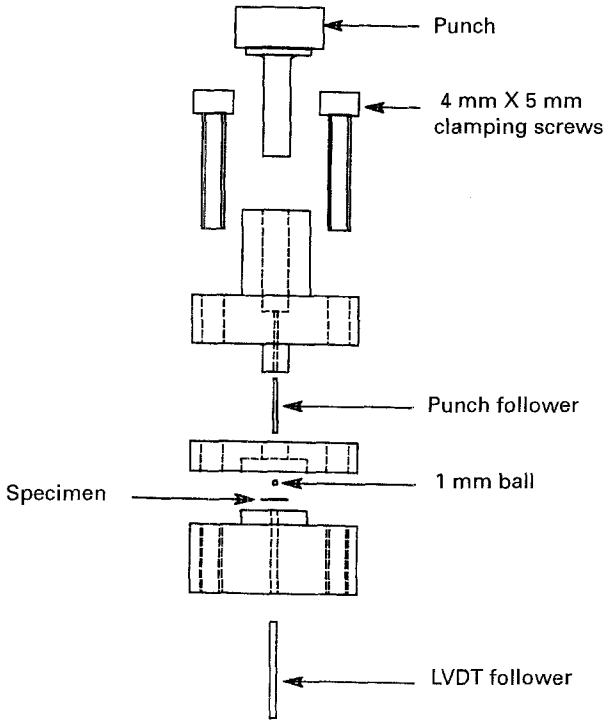

Figure 1 Schematic diagram of the miniaturized disc test jig to test disc specimens 3 mm diameter and 0.25 mm thick.

steel specimens, and in this paper we describe a miniaturized test which uses a 1 mm diameter ball punch applied to measuring the properties of 3 mm diameter, 0.25 mm thick disc specimens of 2¼Cr1Mo steel. The objective was to establish the reproducibility of the test method and analyse the data to obtain a measure of the tensile stress–strain properties, including elastic modulus, yield stress and ultimate tensile strength, together with a simple assessment of the fracture energy over a range of temperature from − 196 to 25 °C.

2. Experimental procedure

2.1. Material

The material used was 2¼Cr1Mo steel with an impurity addition of tin. The chemical composition of the steel is listed in Table I. The material was heat treated at a temperature of 1050 °C for 120 min and then furnace cooled. Specimens were prepared from a rod machined to 3 mm diameter which was sliced into discs ~ 0.4 mm thick. Each disc was then precision ground to the final dimension of 0.25 mm using 800 and 1200 grit silicon carbide paper. The thickness of each specimen was measured using an optical projection system and the deviation in finished thickness of each was accurate to ± 0.005 mm.

2.2. Testing

The miniaturized jig used to test the 3 mm diameter disc specimens is shown schematically in Fig. 1. The main components of the jig are manufactured from Sanderson Kayser KEA 180 high-duty tool steel tempered to a Rockwell hardness of Hr60 to 63 to optimize the tensile strength. The component parts were each machined to a high tolerance, all surfaces being concentric and square to 30 μm, and critical surfaces were ground and polished to a 4 μm finish. The loading ball was a standard 1 mm diameter ball bearing. The experimental configuration uses a non-clamped centre-loaded disc specimen of nominal dimensions 3 mm diameter and 0.25 mm thickness. The upper and lower dies are joined by four screws and this geometry constrains the specimen from cupping upwards at the periphery during testing. The clearance between the specimen and upper die is 0.01 mm. The tensile machine loading bar is fitted with a spherical end to facilitate alignment and the contact area minimized to reduce any possible ice forming on the loading bar during testing.

All tests on the 3 mm diameter disc specimens were performed on a universal testing machine, Hounsfield H10KM, equipped with an environmental chamber cooled with liquid nitrogen. Each test was conducted at a constant crosshead speed of 0.2 mm s^{-1}. Two identical miniaturized disc jigs were used for testing and a cross-correlation was undertaken to ensure no jig-specific bias existed in the resulting data. Temperature was controlled by a chromel/alumel thermocouple positioned in the environmental chamber and a second thermocouple was positioned to measure the temperature of the jig. The tests were performed after a period of about 10 min to ensure the required temperature was achieved. During testing, the load–displacement data were captured at every 4 μm displacement and stored on a microcomputer which allowed the data to be subsequently processed. At each temperature, a minimum of six specimens was tested to ensure an appropriate statistical confidence in the mean value. The stiffness of the testing machine combined with the test jig assembly was measured at room temperature using a linear displacement transducer positioned below the specimen as shown in Fig. 1. This provided an appropriate calibration for this relatively soft system and a correction was applied to each load–displacement curve obtained. This correction factor is particularly important for establishing the initial gradient and overall shape of the load–displacement curve.

3. Calculation of tensile properties from disc specimens

The stress and strain states developed in the miniaturized disc test specimens of 3 mm diameter and

0.25 mm thickness are more complicated than for a simple uniaxial tensile test specimen. We are concerned with bending a small, thin circular plate of material where a biaxial stress state is developed. As a consequence, it is necessary to use solutions appropriate to the elastic regime to derive the uniaxial tensile properties. These are set down in Roake and Young [17] where the mid-surface of the disc specimen is considered to remain unstressed, whereas other points are subject to biaxial stresses in the plane of the disc. This leads to vertical strength lines in the disc becoming inclined when deformed, so that principal stresses at points on these lines are proportional to the distance from the mid-surface and stresses are maximum at the surface of the disc. As a consequence, stresses and strains are not simply related to measured loads and displacements obtained from the miniaturized disc test. We now summarize relationships used to calculate the mechanical properties in this paper based upon the schematic typical load, P, versus displacement, d, curve for a miniaturized disc test shown in Fig. 2.

3.1. Modulus of elasticity

The slope, P/d, of the initial, linear region of the load–displacement curve in Fig. 2 is proportional to the Young's modulus of elasticity, E (GPa). However, the shear and bending displacement for a centrally loaded disc has been analysed and the shear modulus, G, is simply related to the Young's modulus for uniaxial deformation ($G = E/2(1 + \nu)$). As a consequence, E may be calculated using the relationship [15]

$$E = (P/\pi dt)[1.2(1 + \nu)\ln(R/r) + 0.75R^2(1 - \nu^2)/t^2] \quad (1)$$

where t is the specimen thickness, d is the displacement, P is the load, R is the radius of the supporting specimen jig, r is the contact radius, and ν is Poisson's ratio. Equation 1 assumes that the contact radius is constant throughout elastic deformation of the disc and there is no friction at the contact surface. However, because the contact radius increases as the load is increased, this would lead to the evaluated value for E being an underestimate of the true value.

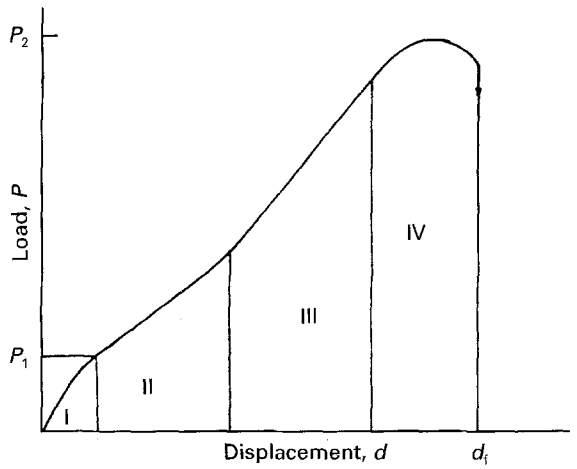

Figure 2 Schematic diagram of a typical load, P, versus displacement, d, curve obtain from small disc specimens [11]. The characteristic deformation behaviour can be divided into four: (I) elastic, (II) plastic, (III) plastic membrane stretching, and (IV) plastic instability. P_1 and P_2 correspond to loads for estimating σ_y and σ_u.

3.2. Yield stress

Values for the yield stress, σ_y, can be calculated from the deviation from linearity of the elastic part of the load–displacement curve, Fig. 2. Because elastic solutions remain valid to this limiting condition, σ_y can be calculated from a knowledge of the applied load, P_1, and the deformation characteristic of a disc specimen [17]. This analysis provides a measure of the tensile stress at the outer surface of a disc below the position of the ball indentor and, for an unconstrained disc, the tensile stress at the periphery. Each stress can be equated to the yield stress, σ_y, and for an unconstrained disc this is given by

$$\sigma_y = [3P_1(1 + \nu)/2\pi t^2][\ln(4R/\pi r_1 + \beta)] \quad (2a)$$

where ν is Poisson's ratio, t is the specimen thickness, β is 0.435 for a disc and

$$r_1 = (1.6r^2 + t^2)^{1/2} - 0.675t \quad \text{for } r < t/2 \quad (2b)$$

and

$$r_1 = r \quad \text{for } r > t/2 \quad (2c)$$

where r is the radius of the contact area between the ball indentor and the disc specimen surface where friction is assumed to be small. For a constrained disc specimen of the type tested in the jig shown in Fig. 1, yielding occurs at the surface where it is supported and under these conditions the relationship for evaluating the yield stress simplifies to [17]

$$\sigma_y = 3P_1/2\pi t^2 \quad (3)$$

It should be noted that Kameda and Mao [18] have proposed an empirical approximation to estimate σ_y for the small punch test procedures based upon a series of experimental data obtained for a range of ferritic steels. This gives a relationship

$$\sigma_y = \alpha P_1/t^2 \quad (4)$$

where α equals 0.36 for low-alloy ferritic steels.

3.3. Strain

For small plastic displacements if we assume the bent disc specimens achieves the shape of a spherical cap, the biaxial tensile strain, ε, is given by [6]

$$\varepsilon = td/(R^2 + d^2) \quad (5)$$

where d is the displacement below the indentor. This equation is obtained from a simple analysis of a bent disc where the radius of curvature is described in terms of the deflection and the support radius. The maximum strain, ε_f, at the lower surface of the disc is obtained by assuming that fracture occurs at the maximum load. This simple approximation is strictly valid only for small displacements because it is under these

conditions that the strain field is approximately uniform. Unfortunately, materials such as ferritic steels, do not behave in this way and this is not a reasonable approximation. Fracture can occur at any displacement beyond the maximum load, P_2, and up to the maximum strain, ε_f (Fig. 2), so that the point of fracture is not simply defined.

3.4. Ultimate tensile strength

In the case of the ultimate tensile strength, σ_u, the larger plastic strains make the translation to the equivalent uniaxial parameter less certain. As a consequence, several analytical and empirical approximations have been developed to derive this parameter. We will consider those that are appropriate to low-alloy ferritic steels. A typical analytical approximation for σ_u is [17, 19]

$$\sigma_u = P_2/22\pi rt \quad (6)$$

where P_2 is the maximum measured load, Fig. 2. However, Kameda and Mao [15, 18] have offered the following empirically derived approximation

$$\sigma_u = \gamma(P_2/t^2) - \eta \quad (7)$$

where γ is 0.13 and η is 0.32 for a range of ferritic steels. Since we are concerned with establishing a uniaxial parameter from the load–displacement data obtained from disc specimens at large strains, the value of σ_u will probably be the least precise estimate of the mechanical properties considered.

4. Results

The microstructure of the $2\frac{1}{4}$Cr1Mo steel specimens containing an impurity addition of tin consists of bainite together with a distribution of coarse $M_{23}C_6$ type carbide precipitates on lath and prior austenite grain boundaries. The specimens have a prior austenite grain size of ~ 100 μm (mean linear intercept). A four-fold increase in the concentration of tin has been measured at the prior austenite grain boundaries on thin-foil specimens using high-resolution X-ray microanalysis [20] as a result of the furnace-cooling heat treatment. The results of uniaxial tensile tests carried out over the temperature range -160 to 25 °C are given in Table II: the test specimens had a gauge length of 20 mm and diameter of 4 mm. Table II gives values for the uniaxial properties, Young's modulus of elasticity, 0.02 proof stress ($\equiv$ yield stress) and ultimate tensile strength.

Typical load–displacement curves obtained for the $2\frac{1}{4}$Cr1Mo steel miniaturized disc test specimens over the temperature range -100 to -190 °C are shown in Fig. 3. At the highest temperature, Fig. 3d, the curve divides into the four characteristic regions shown schematically in Fig. 2: (i) elastic bending, (ii) plastic bending, (iii) plastic membrane stretching, and (iv) plastic instability. The gradient of the initial linear region is used to derive the Young's elastic modulus of the material, E, as given in Section 3. After linear extension, yielding occurs where the yield load, P_1, the position of departure from linearity in the computer-stored data, provides the yield stress, σ_y. This is followed by plastic deformation which propagates radially from the contact area between the ball indentor and the disc specimen. The membrane of the disc specimen continues to stretch until the maximum load, P_2, is reached and this is followed by fracture and ultimate failure of the test specimen. Fig. 3a–d show the change of shape of the load–displacement curves with increasing test temperature. Clearly as the test temperature is reduced plastic deformation becomes progressively restricted and at the lowest temperature (Fig. 3a), yielding is followed rapidly by the onset of brittle fracture and failure of the specimen. In some cases the load–displacement curves did not follow the characteristic shape post-maximum load due to the complexity of disc failure following the onset of fracture. The elastic modulus (Fig. 4), yield stress (Fig. 5a and b), and ultimate tensile strength (Fig. 6a and b), over the range of temperatures at which the tests were conducted, were calculated using the relationships given in Section 3. To assist with these evaluations, the diameter of the contact area between the ball indentor and the disc specimen was measured from visible indentations on the specimens using the optical procedure described by Li *et al.* [5]. For loads less than the yield, the measured indentation diameter varies approximately linearly up to a maximum of 90 μm diameter ($r = 45$ μm) for a room-temperature test. Values of σ_y calculated using the rigorous, Equation 3, and empirical, Equation 4, approximations are compared in Fig. 5a and b. Clearly there is close agreement with the values obtained for uniaxial tests, Table II.

To obtain an estimate of the fracture energy for the $2\frac{1}{4}$Cr1Mo steel, the area under the load–deflection curves was calculated to provide a measure of the total energy to effect fracture of the disc specimens. Fig. 7 shows the variation of this measure of fracture energy, K^*, with test temperature. The mean of the data at each test temperature shows a variation with temperature characteristic of the brittle-to-ductile transition temperature for this $2\frac{1}{4}$Cr1Mo steel. The transition temperature indicated is simply the mid-value between the upper and lower shelf energy, based on mean data. Fig. 8a and b show macrographs of the plastic deformation and crack propagation path within these disc specimens, together with the fracture surface morphology (Fig. 9a and b), at selected temperature positions on the fracture energy plot in Fig. 7. At the lower temperatures there is little evidence of ductility; cracks propagate along radial directions and cleavage fracture is observed. As the

TABLE II Bulk uniaxial mechanical properties for $2\frac{1}{4}$Cr1Mo steel

Temperature (°C)	E (MPa)	$\sigma_{0.02}(\equiv\sigma_y)$ ($\pm$ 20 MPa)	σ_u ($\pm$ 20 MPa)
25	2.14×10^5	311	558
-80	2.28×10^5	362	674
-120	–	436	764
-160	2.41×10^5	539	784

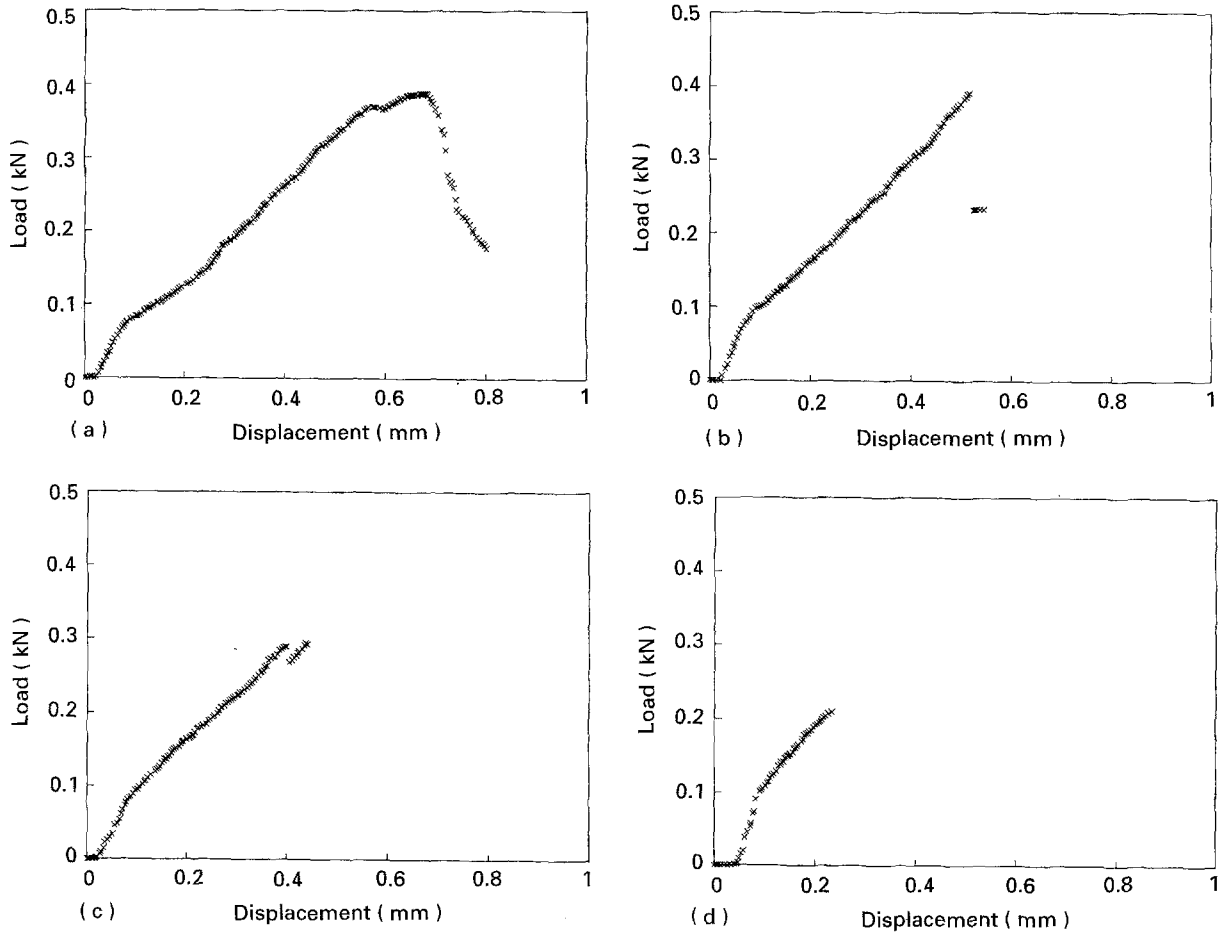

Figure 3 Load–displacement curves obtained for the furnace-cooled 2¼Cr1Mo steel miniaturized disc specimens tested at (a) − 100 °C, (b) − 143 °C, (c) − 170 °C, and (d) − 190 °C.

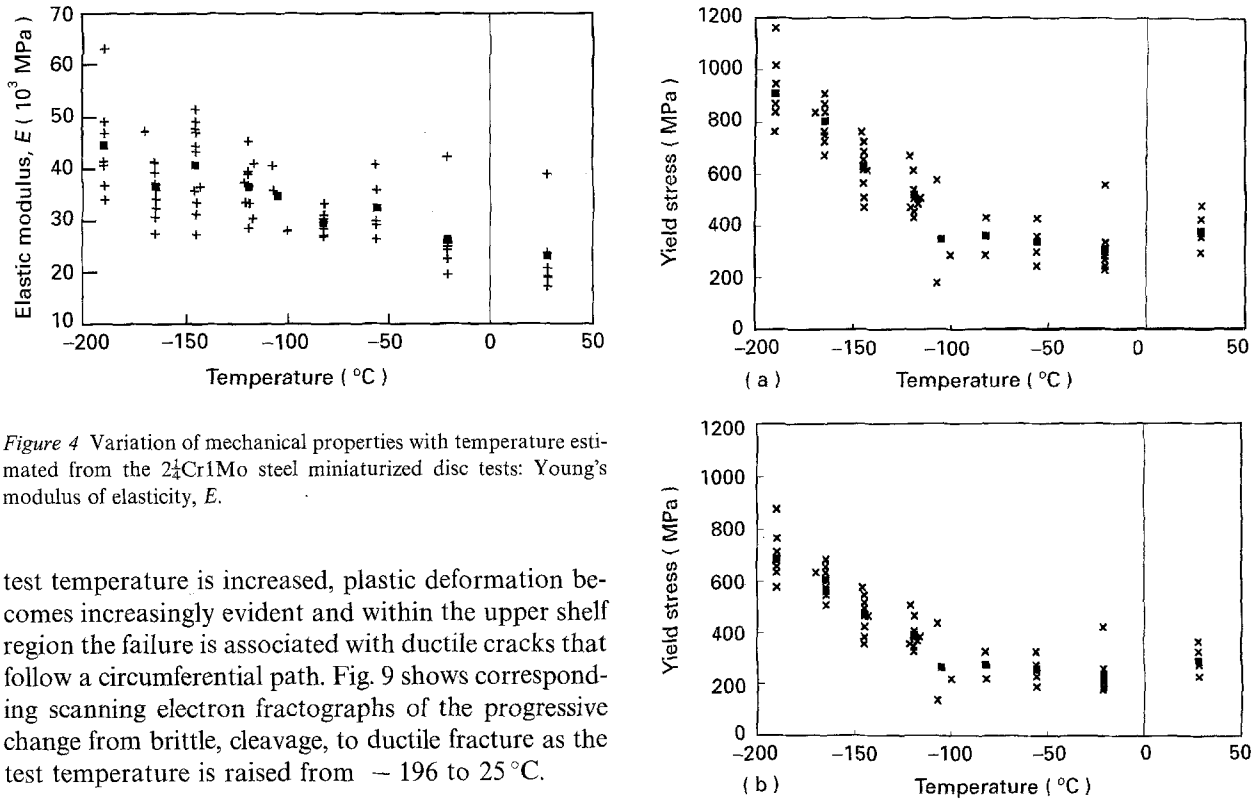

Figure 4 Variation of mechanical properties with temperature estimated from the 2¼Cr1Mo steel miniaturized disc tests: Young's modulus of elasticity, E.

Figure 5 Variation of mechanical properties with temperature estimated from the 2¼Cr1Mo steel miniaturized disc tests: yield stress, σ_y, calculated from the load yield of the load–displacement curves using (a) Equation 3, and (b) Equation 4. (◆), (■) Mean values, respectively.

test temperature is increased, plastic deformation becomes increasingly evident and within the upper shelf region the failure is associated with ductile cracks that follow a circumferential path. Fig. 9 shows corresponding scanning electron fractographs of the progressive change from brittle, cleavage, to ductile fracture as the test temperature is raised from − 196 to 25 °C.

5. Discussion

The disc specimens selected for these miniaturized tests are of a significantly smaller volume than more

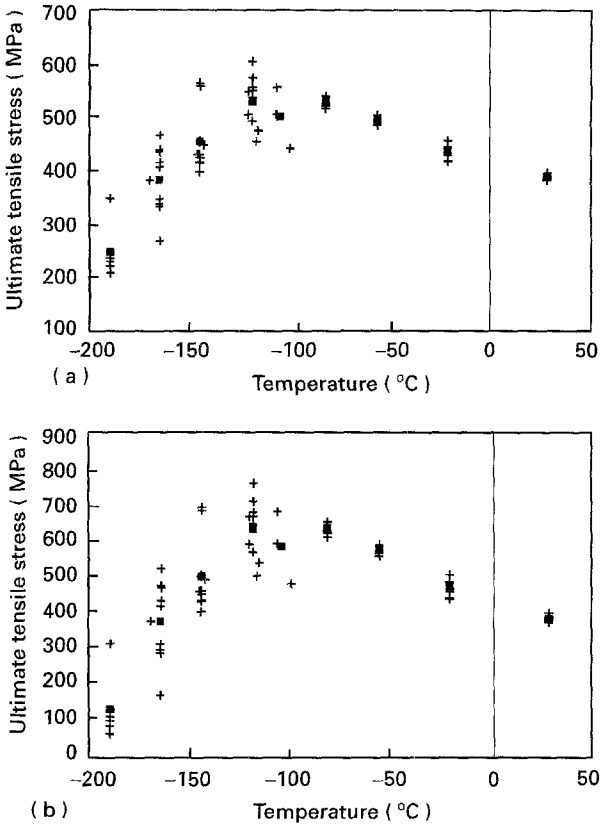

Figure 6 Variation of ultimate tensile strength, σ_u, over the temperature range 25 to $-190\,^{\circ}C$ for $2\frac{1}{4}$Cr1Mo steel disc specimens calculated using (a) Equation 6, and (b) Equation 7.

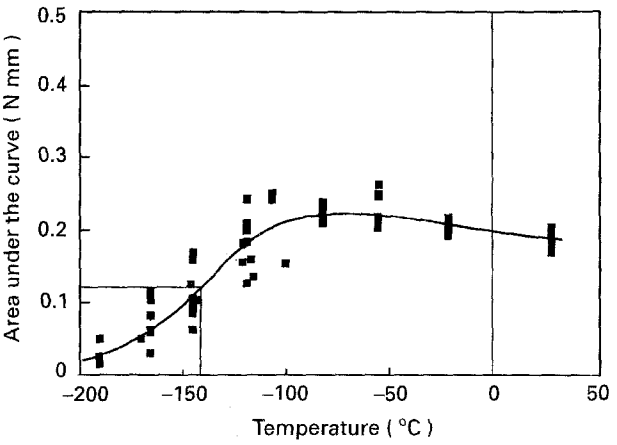

Figure 7 Variation of fracture energy, K^*, estimated from the miniaturized disc specimens of $2\frac{1}{4}$Cr1Mo steel with temperature.

conventional test specimens used to measure mechanical properties. Indeed they are at least an order of magnitude smaller than many specimens used in tests classed as "small specimen". As a consequence of both the small size of specimen and the volume of material sampled, there is the potential for introducing substantial random errors into the finally produced data that could prevent a realistic measure of mechanical property parameters. The sources of potential error are associated with (i) the specimen, (ii) the testing method, and (iii) the collection and interpretation of the data.

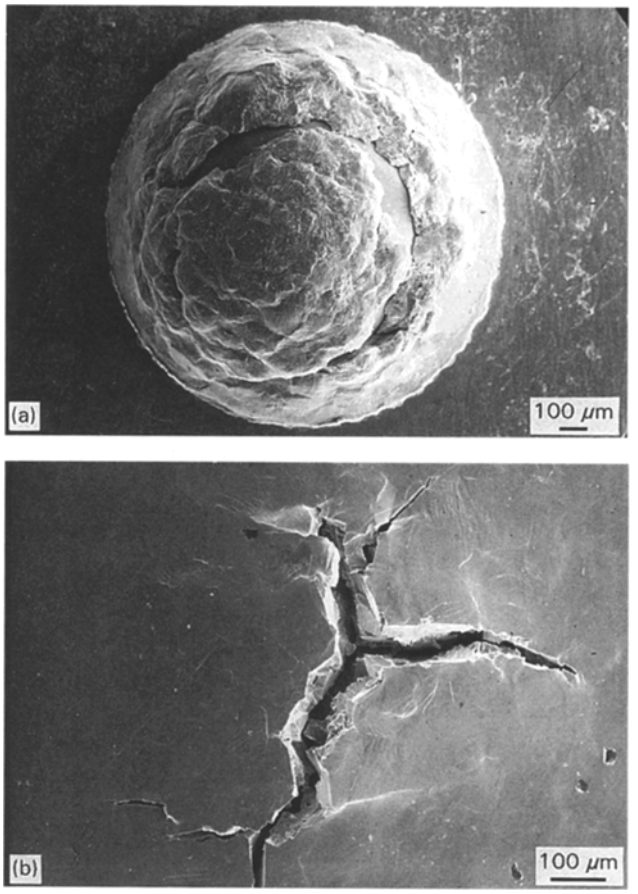

Figure 8 Low-magnification scanning electron micrographs of the failed disc specimens of $2\frac{1}{4}$Cr1Mo steel showing the plastic deformation and crack propagation paths at temperatures of (a) 25 °C, and (b) $-190\,^{\circ}C$.

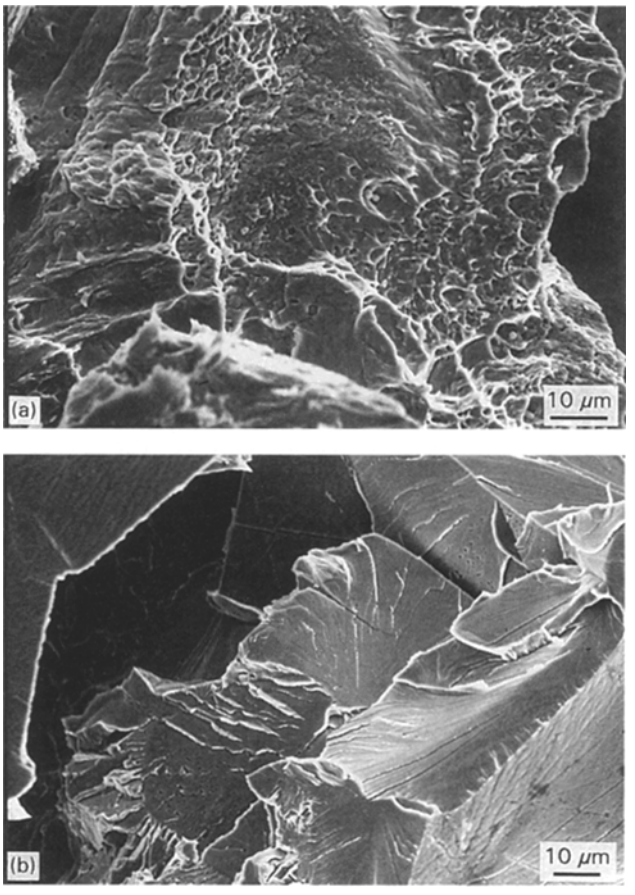

Figure 9 Scanning electron micrographs (secondary electron mode) of the fracture surfaces of the $2\frac{1}{4}$Cr1Mo test specimens shown in Fig. 8 at temperatures of (a) 25 °C, and (b) $-190\,^{\circ}C$.

With the small size of the disc specimen it is important that the material selected is representative of the whole body. In the present $2\frac{1}{4}$Cr1Mo steel the composition and microstructure are relatively uniform, which reduces the potential for this source of error. Furthermore, it is essential to prepare the disc specimens to a consistent and reproducible geometry and surface finish. The scatter observed in the present results (Figs 4–8) show that the thickness control on the discs to within ± 0.005 mm, or $\pm 2\%$, is sufficient, provided an adequate surface finish is achieved. Following a series of trials, a standard 1200 grit finish provided this consistency. The surface finish is particularly important for these bend geometry specimens because the strain is a maximum at the surface (see Section 3). Indeed Li *et al.* [5] have shown that it is possible to measure properties local to the surface using disc specimens of amorphous $Fe_7Si_9B_{13}$ melt-spun ribbons.

The test jig described in Section 2 and used for the present work has been manufactured to very strict machining tolerances. However, there are three potential contributions that can lead to misalignment in the test system and therefore error: (i) coincidence between the punch and die axes of symmetry, (ii) machining tolerances for each component part of the jig assembly, and (iii) centring of the disc specimen within the jig. The first two were confirmed to be acceptably small by the use of two jigs manufactured to the same tolerances and surface finish where the results do not show a bias between the two. In the case of specimen positioning within the jig, this was measured to be within a circle of 0.1 mm diameter of the centre representing a positional error of up to $\sim 3\%$. By inspection of the yield stress data in Fig. 5a and b, the spread in the data represent a reproducibility in the measured value of typically $\pm 20\%$ of the mean. This is larger than the cumulative value for the major sources of error, but is not inconsistent with that anticipated or acceptable from such a test when material variability is included.

From a basic understanding of the responses of different regions of the load–displacement curves for the miniaturized disc specimens (Figs 2 and 3), it has been possible to estimate equivalent uniaxial properties (Section 3). The acquisition of the test data was ensured by computer storage and this has afforded the capability to process the data and derive the Young's elastic modulus, yield stress, ultimate tensile strength and area under the load–displacement curves using the equations set down in Section 3.

Unfortunately, the Young's modulus of elasticity is not an easy parameter to measure, even from a simple uniaxial tensile test, Table II. The values of the modulus of elasticity, E, derived from the present tests on disc specimens are subject to further error. The stiffness of the complete test system adopted has been measured and is used as a correction to obtain the finally evaluated modulii. However, the values shown in Table II for this $2\frac{1}{4}$Cr1Mo steel over the temperature range for the tests are in reasonable agreement with reported bulk values [21]. Because the elastic modulus is determined by the interatomic forces in the material it is not a very structure-sensitive mechanical property. However, variation of modulus with temperature for the values obtained from the disc specimens, Fig. 4 is consistent with the measured trend, Table II. Values obtained from the miniaturized disc tests tend to be smaller than the bulk values by a factor of four or five. Partly this error can be accounted for by the assumptions in Equation 1 that the radius of the contact area between the ball indentor and the disc remains constant, contact is frictionless and shear modulus translates simply to E for deforming a disc specimen. This is coupled with a cubic specimen thickness dependence which will enhance the contribution from small differences in the original thickness of the specimens. It is noteworthy that although the absolute values are smaller, the temperature dependence is in good agreement with the uniaxial data in Table II.

Comparison of the yield stress for disc specimens has been estimated from departure of the initial linearity of the load–displacement curve point, P_1 (Fig. 2). The general form of the load–displacement curves measured, (Fig. 3), are consistent with those predicted by a finite element code described by Hanling *et al.* [22]. The results over the full temperature range of the tests show the variation of yield stress with temperature which is anticipated for this ferritic steel and which is in agreement with the data in Table II. In Fig. 10 we compare the results for σ_y obtained using the analytical solution, Equation 3, for a deforming membrane [17] and the empirical relationship, Equation 4, obtained for a range of ferritic steels [15, 18] with the uniaxial data. The basis of the comparison is the 0.2% proof stress because there is no defined yield point in this material. The values derived by both methods are in good agreement with the bulk values, but the best fit is obtained from the empirical solution, Equation 4, and it is recommended that this be used for future methods for deriving the yield stress for low-alloy ferritic steels. The values of ultimate tensile strength (Fig. 6a and b) obtained from a measure of P_2 (Fig. 2) are in reasonable agreement with bulk values for this steel. It is not anticipated this will provide anything but an approximate estimate, because the disc specimen will be subject to significant plastic strain and therefore a more rigorous elastic/plastic analysis would be required rather than the simple relationships adopted. Moreover, it is evident that at temperatures below about $-150\,^{\circ}C$, the methods described in Section 3 for calculating σ_u are no longer valid.

Finally, we turn to the measure of the brittle-to-ductile transition temperature based upon the plot of the miniaturized disc test fracture energy, K^*. Clearly the results in Fig. 7 show that it is possible to obtain a change of K^* with test temperature and this follows the form of curve with temperature traditionally observed for Charpy impact energy and valid fracture toughness tests. Since fracture can occur at any value of displacement beyond point P_2 shown in Fig. 2 to the end of the load–displacement curve, ε_f, an arbitrary criterion for establishing the area under this curve to derive K^* has been adopted; this will

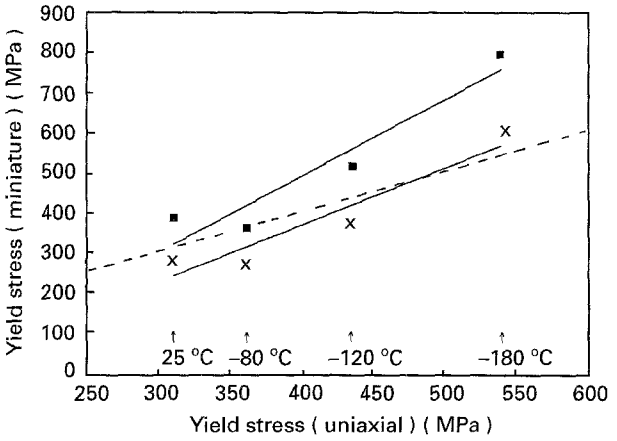

Figure 10 Comparison of the yield stress, σ_y, determined from the miniaturized disc specimen test compared with the bulk uniaxial values. (– – –) Gradient = 1; (———) regression fit to data, (■) Equation 3, (×) Equation 4.

introduce an additional but consistent uncertainty into the data. However, the results given in Fig. 7 show that a transition temperature can be derived from the mean of each data set at a given test temperature. As with other data obtained by this method the transition temperature obtained from K^* values is significantly displaced to lower temperatures when compared with a traditional transition temperature based upon Charpy impact energy, fracture appearance or fracture toughness. As a consequence, an empirically derived conversion factor would have to be obtained to estimate equivalent bulk values to be evaluated. This is not surprising because in the case of Charpy and fracture toughness test specimens, the size and geometry define the constraint which directly affects the brittle-to-ductile transition.

The present results do show positive and useful features that provide a basis for extending the analysis to derive a measure of the brittle-to-ductile transition temperature. First the fracture mechanism clearly changes from brittle cleavage, associated with lower test temperatures, to fully ductile at the higher test temperatures, Figs 8 and 9. In addition, Fig. 7 shows a change in the magnitude of the standard deviation of the data at each test temperature. At low and high temperatures, where there is a single fracture mode, either cleavage or ductile, the standard deviation is small. However, within the transition region this increases significantly reflecting the competition between the two fracture processes. This provides a basis for quantifying the transition temperature which is developed by the authors elsewhere [23].

6. Conclusions

1. A method is described which produces reproducible test data using a miniaturized disc test specimen, 3 mm diameter and 0.25 mm thick.

2. Despite the various sources of error associated with testing small disc specimens, realistic estimates have been obtained of the equivalent bulk mechanical properties, the Young's modulus of elasticity, yield stress and ultimate tensile strength for a $2\frac{1}{4}$Cr1Mo steel over the temperature range – 196 to 25 °C.

3. A measure of the total energy to fracture, K^*, for the miniaturized disc test is derived and this varies with temperature, showing cleavage fracture at the lower test temperatures and ductile fracture at the higher temperatures.

Acknowledgements

The authors thank Mr R. F. Smith and Mr P. Bennet for their considerable assistance with the test procedures, and Mr P. J. Fielding and Dr R. Moskovic for helpful discussions. This paper is published with the permission of the Director, Technology Division, Nuclear Electric plc.

References

1. P. E. J. FLEWITT, G. H. WILLIAMS and M. B. WRIGHT, *Nucl. Energy* **31** (1992) 383.
2. C. A. ENGLISH, A. J. FUDGE, R. J. McELROY, W. J. PHYTHIAN, J. T. BUSWELL, C. J. BOLTON, P. J. H. HEFFER and R. B. JONES, *Int. J. Press. Vess. Piping* **54** (1993) 49.
3. N. H. PACKAN, R. E. STOLLER and A. S. KUMAN (eds), "Effects of Radiation on Materials", ASTM STP 1046 (American Society for Testing and Materials, Philadelphia, PA, 1990).
4. G. E. LUCAS, *Metall Trans.* **21A** (1990) 1105.
5. H. LI, F. C. CHEN and A. J. ARDELL, *ibid.* **22A** (1991) 2061.
6. F. M. HUANG, M. L. HAMILTON and C. L. WIRE, *Nucl. Technol.* **57** (1982) 234.
7. M. P. MANAHAN, A. S. ARGON and O. K. HANLING, *J. Nucl. Mater.* **103–104** (1981) 1545.
8. G. E. LUCAS, J. W. SHECKHERD, G. R. ODETTA and S. PANCHANADEESWARAN, *ibid.* **122–123** (1984) 1040.
9. T. M. CHANG, *J. Inst. Metals* **78** (1950) 393.
10. A. G. ATKINS, *Int. J. Mech. Soc.* **22** (1980) 215.
11. J. M. BAIK, J. KAMEDA and O. BUCK, "The Use of Small-Scale Specimens for Testing Irradiated Material", STP 888 (American Society for Testing and Materials, Philadelphia, PA, 1986).
12. X. MAO, T. SHOJI and H. TAKAHASHI, *J. Test. Eval.* **15** (1987) 15.
13. T. MISAWA, T. ADACHI, M. SAINTO and Y. HAMAGUCHI, *J. Nucl. Mater.* **150** (1987) 194.
14. J. McNANCY, G. E. LUCAS and G. R. ODETTA, *ibid.* **179–181** (1991) 429.
15. J. KAMEDA and X. MAO, *Mater. Sci. Eng.* **A122** (1989) 143.
16. L. F. EXWORTHY, Nuclear Electric Memorandum, TD/SEB/MEM/2274/91 (1991).
17. R. J. ROAKE and W. C. YOUNG, "Formulas for Stress and Strain", 6th Edn (McGraw-Hill, New York, 1980) p. 391.
18. J. KAMEDA and X. MAO, *J. Mater. Sci.* **27** (1992) 983.
19. X. MAO and H. TAKAHASHI, *J. Nucl. Mater.* **50** (1989) 42.
20. V. VORLICEK and P. E. J. FLEWITT, *Acta Metall. Mater.* **42** (1994) 3309.
21. M. HOLZMANN, B. VLACH, J. MAN and Z. BILEK, *Int. J. Pres. Vess. Piping* **36** (1989) 125.
22. O. K. HANLING, M. LEE, D.-S. SOHN, E. KOHSE and C. W. LAN, "Use of Small Scale Specimens for Testing Irradiated Material" ASTM STP 888 (American Society for Testing and Materials, Philadelphia, PA, 1983) p. 50.
23. V. VORLICEK, R. MOSKOVIC and P. E. J. FLEWITT, to be published (1993).

Received 6 September 1993
and accepted 5 July 1994